THE JOURNAL OF PHYSICAL CHEMISTRY A

Article

pubs.acs.org/JPCA

Photophysics of Ru(II) Dyads Derived from Pyrenyl-Substitued Imidazo[4,5-*f*][1,10]phenanthroline Ligands

Christian Reichardt,[†,‡] Mitch Pinto,[§] Maria Wächtler,[‡] Mat Stephenson,[§] Stephan Kupfer,[†] Tariq Sainuddin,[§] Julien Guthmuller,[∥] Sherri A. McFarland,*[,§] and Benjamin Dietzek*[,†,‡]

[†]Institute of Physical Chemistry and Abbe Center of Photonics, Friedrich-Schiller-University Jena, Helmholtzweg 4, 07743 Jena, Germany

[‡]Leibniz Institute of Photonic Technology (IPHT) e.V., Albert-Einstein-Straße 9, 07745 Jena, Germany

[§]Department of Chemistry, Acadia University, Wolfville, NS B4P 2R6, Canada

[∥]Gdansk University of Technology, Narutowicza 11/12, 80-233 Gdansk, Poland

Supporting Information

ABSTRACT: The photophysics of a series of Ru(II) dyads based on the 2-(1-pyrenyl)-1*H*-imidazo[4,5-*f*][1,10]-phenanthroline ligand was investigated. The ability of these metal complexes to intercalate DNA and induce cell death upon photoactivation makes them attractive photosensitizers for a range of photobiological applications, including photodynamic therapy. In the present study, time-resolved transient absorption and emission spectroscopy were used to interrogate the photoinduced processes that follow metal-to-ligand charge transfer excitation of the complexes in solution. It was found that energy transfer to pyrene-localized intraligand triplet states, facilitated by torsional motion of the pyrene moiety relative to the imidazo[4,5-*f*][1,10]phenanthroline ligand, was an important relaxation pathway governing the photophysical dynamics in this class of compounds. Biphasic decay kinetics were assigned to spontaneous (pre-equilibrium) and delayed emission, arising from an equilibrium established between ^{3}MLCT and ^{3}IL states. TDDFT calculations supported these interpretations.

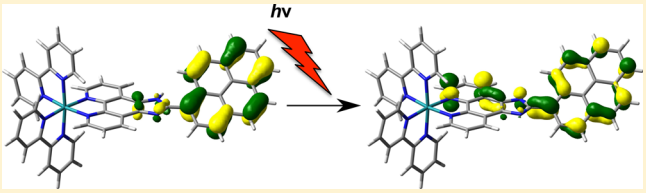

1. INTRODUCTION

The significant role of ruthenium(II) polypyridyl complexes in contemporary photochemistry is related to their rich photophysical and electrochemical properties, which make these transition metal compounds attractive as photosensitizers (PSs) for molecular devices,[1−3] dye-sensitized solar cells,[4−6] photocatalysts (i.e., water splitting[7−9] or artificial photosynthesis[9,10]), and luminescence sensors.[11−13] They are also of interest as biomedical diagnostics and pharmaceuticals and as phototherapy agents.[14−19] The intense focus that Ru complexes have received, from photovoltaics to photomedicine, is due at least in part to their modular scaffolds that afford the opportunity to access a wide variety of excited state configurations through rational design. Such states include metal-to-ligand charge transfer (MLCT), metal-centered (MC), ligand-centered (LC) or intraligand (IL), intraligand charge transfer (ILCT), ligand-to-ligand charge transfer (LLCT), metal-to-metal charge transfer (MMCT), and others.

Of importance to phototherapy applications in particular are states that can (i) sensitize singlet oxygen ($^1O_2$) through type II energy transfer, (ii) participate in type I electron transfer processes to form reactive intermediates, (iii) undergo type III redox chemistry directly with cellular targets, and (iv) form covalent adducts with biomolecules such as DNA via ligand dissociation or other photochemical reactions. Nominally, type I−III photoprocesses have been referred to as photodynamic in nature (especially when they involve oxygen or reactive oxygen species (ROS), and classified as photodynamic therapy (PDT)[20−22] when these reactions are employed to destroy cells. In contrast, the term photoactivated cancer (or chemo) therapy (PACT)[23] has emerged to describe cytotoxicity invoked with class (iv) photochemical agents. In practice, photoprocesses i−iv are not mutually exclusive, and more than one configuration may be involved in generating phototherapeutic effects. The Ru(II) compounds that are the subject of this investigation act as potent PSs, destroying both cancer and bacterial cells in the nanomolar regime, and may be classified as PDT (or phototherapy) agents since previous studies show that they do not undergo ligand loss from dissociative ^{3}MC states upon photoexcitation.[24] These complexes belong to a class of compounds that we call metal−organic dyads, and their unusual PDT effects stem from low-energy ^{3}IL states contributed by organic chromophores.

Metal−organic dyads merge the best features of inorganic and organic chromophores by appending a metal complex with a π-expansive organic unit either tethered to or contiguously fused with one of the metal chelating ligands. These hybrid arrangements produce low-lying triplet IL configurations that

Received: February 26, 2015
Revised: March 31, 2015
Published: March 31, 2015

DOI: 10.1021/acs.jpca.5b01737
J. Phys. Chem. A 2015, 119, 3986−3994

are in energetic proximity to MLCT states. While the photophysics and photochemistry of traditional Ru(II) polypyridyl complexes is thought to be set by the relative energies of thermalized ^{3}MC and ^{3}MLCT states, low-lying ^{3}IL states can completely alter the excited state profiles of these systems by prolonging triplet excited state lifetimes and increasing excited state reactivity through ^{3}IL-^{3}MLCT equilibration or population of pure ^{3}IL states.

Unlike organic compounds, metal complexes undergo spin−orbit coupling (SOC) with high efficiency (almost 100%) to form photosensitizing triplet states with visible-light activation. Triplet state formation in pure organics requires shorter-wavelength excitation and is far less than unity, reducing the number of excitions that can produce cytotoxic $^1O_2$ or other reactive species with low-energy light. Nevertheless, once formed, organic triplets have very long intrinsic lifetimes that make them extremely sensitive to bimolecular quenchers. By contrast, facile SOC in metal complexes shortens triplet state lifetimes relative to pure organics ($[Ru(bpy)_3]^{2+}$, τ (77 K) ≈ 5 μs vs 700 ms for pyrene),[25] reducing the time for bimolecular encounters. Ru dyads simultaneously exploit the large quantum yields for triplet state formation with visible light in metal complexes (large singlet−triplet SOC) and the long intrinsic triplet lifetimes of organic arenes (small triplet-singlet SOC), giving rise to constructs that exhibit the longest reported lifetimes for Ru(II) complexes (270 μs in deoxygenated MeCN and 3.44 ms at 77 K in alcoholic glass) with unprecedented sensitivity to oxygen.[26] These first-reported pyren-1-ylethynyl-1,10-phenanthroline (PEP)-derived Ru dyads exhibited nanomolar light cytotoxicities for in vitro PDT against human leukemia cells and notoriously hard-to-kill metastatic melanoma cells, with the largest known phototherapeutic indices (PIs) (>1700). Such potency was attributed to lowest-lying, pure ^{3}IL states that do not thermally equilibrate with ^{3}MLCT states.

In order to explore the scope of ^{3}IL states in other metal−organic hybrids, we recently investigated Ru(II) dyads derived from 2-(1-pyrenyl)-1*H*-imidazo[4,5-*f*][1,10]phenthroline (ippy) as versatile PSs for generating the PDT effect against cancer cells and photodynamic inactivation (PDI) of bacteria.[24] These complexes proved to be sensitive to trace amounts of oxygen (K_{SV} as low as 0.2393 Torr^{-1}),[27] making them attractive PSs for targeting hypoxic tumors with PDT. There is much interest in the design of oxygen-independent PSs for PDT given that the most aggressive and drug-resistant malignancies are hypoxic.[28,29] Like their PEP counterparts, Ru ippy dyads exhibited nanomolar light cytotoxicities with large PIs, but this activity was slightly attenuated. The Ru ippy dyads were also activatable with red light where their molar extinction coefficients were quite small (>100 M^{-1} cm^{-1}), and exhibited the DNA light-switch effect[30−32] with K_b between 1.7 and 8.0 × 10^6 and emission enhancements greater than 10-fold. Notably, the coligands could be varied to control the degree of dark toxicity according to lipophilicity, thus rationally controlling PI values. With less lipophilic ligands (such as bpy and phen), Ru ippy dyads exhibited light-dependent cellular uptake, an important property for suppressing genotoxic and cytotoxic effects in healthy tissue outside the irradiation window.

Resonance Raman experiments confirmed that the longest-wavelength ^{3}MLCT transition involved ippy as the acceptor ligand, and biphasic relaxation kinetics revealed dual emission that was assigned to ^{3}MLCT pre-equilibrium, or spontaneous, emission (τ_1 ≈ 1 μs) and delayed ^{3}MLCT emission (τ_2 > 50 μs) arising from an excited state equilibrium between ^{3}MLCT and ^{3}IL states. The longer lifetime could not be isolated as a distinct state with ^{3}IL spectral characteristics using gated methods or at 77 K. In fact, solid matrices produced monoexponential emission decays from the Ru ippy dyads on the order of 5−10 μs, suggesting that ^{3}IL states were inaccessible in rigid media. Given that thermalized ^{3}MLCT energies were estimated at 1.9−2.0 eV for Ru ippy dyads with typical diimine ligands (2,2′-bipyridine (bpy), 1,10-phenanthroline (phen), etc.) and that conjugated pyrene $\pi\pi^*$ states lie near 2.0 eV, we hypothesized that some degree of torsional motion about the coannular bond joining imidazo[4,5-*f*][1,10]-phenanthroline (ip) and pyrene may accompany population of ^{3}IL states from roughly isoenergetic ^{3}MLCT states.

In this study, Ru dyads **1**−**4** (Figure 1) of the type $[Ru(LL)_2(ippy)]^{2+}$, with LL = bpy, phen, 4,4′-dimethyl-2,2′-bipyridine (dmb), or 4,4′-di-*tert*-butyl-2,2′-bipyridine (dtbb), respectively, were investigated on submicrosecond timescales with emission and transient absorption spectroscopy. Our goal was to gain a better understanding of the excited state dynamics that lead to ^{3}MLCT-^{3}IL equilibration in aqueous environments in order that we might optimize the PDT effect in these systems. Furthermore, these studies will form the basis for future investigations aimed at delineating how these photoinduced processes are influenced by interactions with DNA.

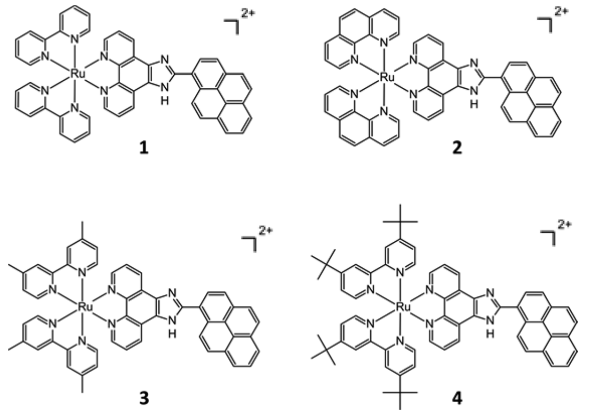

Figure 1. Structures of the four Ru(II) complexes investigated in this study.

2. EXPERIMENTAL AND COMPUTATIONAL SECTION

Compounds **1**−**4** (Figure 1) were prepared as previously described.[24] Steady-state and femtosecond time-resolved spectroscopic experiments were performed at room temperature in air-equilibrated spectroscopic-grade solvents (Sigma-Aldrich). For nanosecond transient absorption measurements, the solvents were deaerated by the freeze−pump−thaw method to remove oxygen. Complexes **1**−**3** were dissolved in distilled water, while **4** was supplemented with 5% v/v dimethyl sulfoxide (DMSO) for complete dissolution.

Steady-state absorption spectra were recorded using a Jasco V-670 spectrophotometer on samples prepared in a quartz cell with a 1 cm path length.

Nanosecond transient absorption and emission lifetime measurements of compound **1** were performed in water in a sealed quartz cell with 1 cm path length (OD = 0.5 at 410 nm) on a commercially available system from Pascher Instrument AB that has been described previously.[24] Samples were excited with 10 ps pulses centered at 410 nm. For transient absorption

DOI: 10.1021/acs.jpca.5b01737
J. Phys. Chem. A 2015, 119, 3986−3994

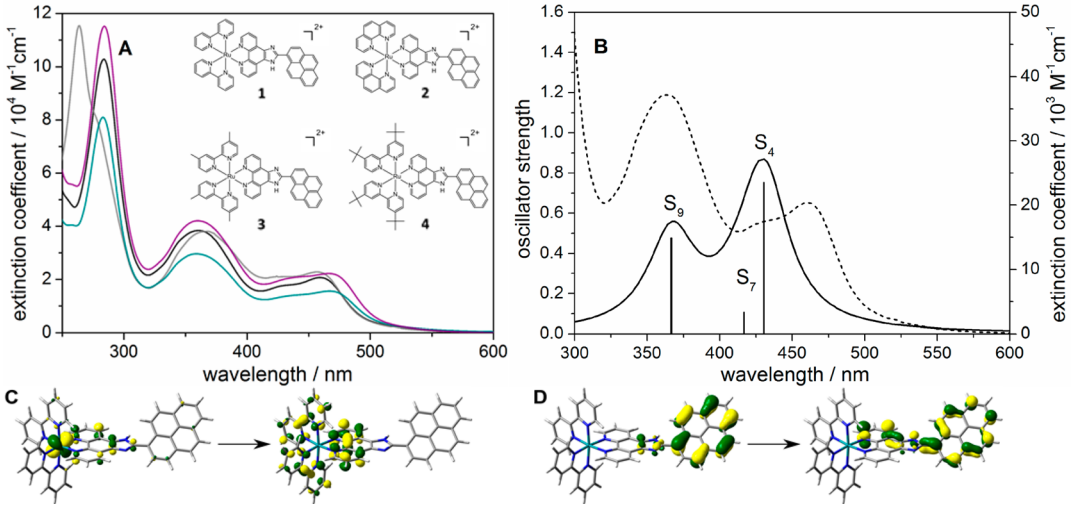

Figure 2. (A) Experimental absorption spectra of **1** (black), **2** (gray), **3** (cyan), and **4** (violet) in water at pH 7. (B) Experimental (dashed) and calculated (solid) absorption spectra of **1** (see SI for more details). The calculated oscillator strengths are represented by black bars. A Lorentzian function with a full-width at half-maximum (fwhm) of 2500 cm^{-1} was employed to broaden the transitions in the simulated spectrum. Donor and acceptor molecular orbitals involved in excitation at (C) MLCT (centered at 465 nm) and (D) IL band (centered at 370 nm) of **1**.

measurements, the probe wavelength was scanned between 380 and 800 nm in steps of 10 nm, and a quantitative data analysis was based on a global fit of the data obtained at all probe-wavelengths. Emission lifetimes were recorded at 600 nm using the ns-transient absorption system without the probe light.

The setup for femtosecond transient absorption is described elsewhere.[33,34] Samples **1**−**4** were excited at 403 nm (compound **1** was also excited at 483 nm). The photoinduced dynamics were probed with a white-light supercontinuum. Samples were added to a quartz cell (1 mm path length), with the final concentrations of the complexes adjusted to yield an optical density of approximately 0.5 at the corresponding excitation wavelength. The data was chirp-corrected and subsequently analyzed by a global fitting routine using a sum of exponential functions. For solvent viscosity- and polarity-dependent measurements, **1** was dissolved in solvents with varying viscosity and polarity: acetonitrile (ACN; ε = 35.7, η = 0.39 mPa·s), butyronitrile (BCN; ε = 24.3, η = 0.57 mPa·s), DMSO (ε = 40.68, η = 2.14 mPa·s), and 1,3-dimethyl-3,4,5,6-tetrahydro-2(1*H*)-pyrimidinone (DMPU; ε = 36.1, η = 2.93 mPa·s).

Sample integrity was ensured throughout all time-resolved spectroscopic experiments by recording absorption spectra of the samples before and after each spectroscopic experiment. No spectral changes indicative of sample degradation were observed.

The structural and electronic data of **1** was obtained from quantum chemistry calculations using Gaussian 09. The geometry, vibrational frequencies, and normal coordinates of the respective ground states were calculated by DFT with the exchange-correlation (XC) functional B3LYP,[35,36] B3LYP35,[37] a functional based on B3LYP combining 35% of exact exchange, 58.5% of nonlocal B88[38] exchange and the LYP correlation, and CAM-B3LYP.[39] The 28-electron relativistic effective core potential MWB[40] was used with its basis set for the Ru atom, that is, 4s, 4p, 4d, and 5s electrons are treated explicitly, whereas the three first inner shells are described by the core pseudopotential. The 6-31G(d) double-ζ basis set[41] was employed for the ligands. The vertical excitation energies and oscillator strengths of the excited states were obtained from TDDFT calculations within the adiabatic approximation with the same XC functionals (B3LYP, B3LYP35, and CAM-B3LYP), pseudopotential, and basis set. To gain insight into the relaxation pathways of **1** upon excitation, the lowest triplet state was optimized at the TDDFT level. Subsequently, the potential energy surface along the dihedral angle δ, describing the torsion with respect to the imidazole and the pyrene fragment, was calculated between $-55° \leq \delta \leq +55°$ and with a step size of 1°.

3. RESULTS AND DISCUSSION

3.1. Steady-State Absorption. For imidazole-containing ligands, it has been shown that the protonation state of the imidazole ring significantly impacts the photophysical properties of both the isolated ligands[42−44] and their respective transition metal complexes.[45−47] Three protonation states are possible for compounds **1**−**4**: the cationic protonated imidazole ring, and its neutral and anionic counterparts. UV/vis titration experiments in water were performed on **1** (see the Supporting Information, SI) as a model system for series **1**−**4**, which differ only in the identity of the coligands. While all three protonation states could be accessed over the pH range of the titration, the neutral form of **1** predominated at pH 7 and is, therefore, considered to be the relevant form of **1**−**4** in this photophysical study.

The absorption spectra of **1**−**4** in water (Figure 2A) displayed characteristic MLCT transitions in the visible region, centered at 465 nm (Table 1). IL transitions contributed to the absorption spectrum near 275 and 370 nm. Based on the calculated absorption spectrum of **1** in water (Figure 2B), the MLCT band corresponds to a mixture of Ru ($d\pi$) → ippy, bpy/phen (π^*) transitions, while the IL band centered at 370 nm can be assigned to the $\pi \rightarrow \pi^*$ transitions of the ippy ligand (molecular orbitals shown in Figure 2C,D). Compound **2** showed a high energy IL transition at 262 nm, attributed to $\pi \rightarrow \pi^*$ transitions of the phen ligand,[48] while the analogous bpy ligand transitions for **1**, **3**, and **4** occurred at 284 nm.

3.2. Nanosecond Transient Absorption. Time-resolved, selected-wavelength transient absorption kinetics in the ns-μs regime were previously reported for **1** in water.[24] In this contribution, the spectral characteristics for **1**−**4** were

DOI: 10.1021/acs.jpca.5b01737
J. Phys. Chem. A 2015, 119, 3986−3994

Table 1. Photophysical Parameters Determined for 1−4 in Water[a]

compound	λ_{MLCT}/ nm	ε (λ_{MLCT})/ M^{-1} cm^{-1}	τ_1/ ps	τ_2/ ps	τ_3/ μs	τ_{em1}/ μs	τ_{em2}/ μs
1	459	20700	2.2	33	52	0.6	26
2	457	22800	1.7	21	50	1.1	26
3	467	15600	2.9	24	51	0.8	23
4	467	22200	3.1	27	49	1.2	26

[a]Transient absorption time constants were obtained by global fit of the femtosecond time-resolved absorption data with two exponential functions and an infinite component and for nanosecond time-resolved absorption data with mono-exponential function. Emission lifetimes were obtained at a probe wavelength of 600 nm.

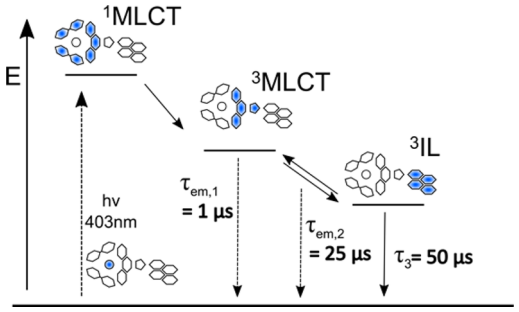

Figure 4. Schematic representation of the relative energetic positioning of the excited states involved in the μs excited state dynamics of **1**.

investigated in more detail with ns transient absorption (Figure 3A exemplary for **1**). The spectral shape of the transient data on the μs timescale consisted of a ground state bleach (GSB) below 400 nm and positive ΔOD values beyond 400 nm, representing excited state absorption (ESA) with a maximum around 550 nm. At all probe wavelengths and for all compounds, the decay of the ESA was monoexponential with a time constant τ_3 of around 50 μs (Table 1) and was accompanied by a concerted recovery of the ground state (Figure 3B).

Further important information about ground-state recovery can be gleaned from the emission lifetimes of **1**−**4** (Figure 3C). Biexponential decay kinetics were observed for all of the compounds (Table 1). The short component τ_{em1} was approximately 1 μs and can be assigned to spontaneous emission originating from the ^{3}MLCT state. In a previous study, the emission lifetime of the core complex without the pyrene substituent was determined to be 462 ns.[49] The spectral similarities between the unsubstituted complex and **1**−**4** suggest that both emission components originate from a common excited state, with the long-lived component assigned to delayed luminescence from the ^{3}MLCT state. It is the relatively small energy gap between the thermalized ^{3}MLCT state and the ^{3}IL (pyrene) state that leads to an excited-state equilibrium between these configurations.[50] Figure 4 summarizes this deactivation pathway exemplary for **1**, and demonstrates the impact of low-lying ^{3}IL states on the photophysics of these complexes. As we have shown previously, prolonging excited-state lifetimes with judicious placement of ^{3}IL states has important implications in the design of PSs for PDT.[24,51]

3.3. Femtosecond Transient Absorption. The ns experiments shed light on the decay of the investigated systems, but not the formation of their excited states. Therefore, fs transient absorption spectroscopy was used to achieve the time resolution necessary to interrogate the processes leading to the photoinduced population of the ^{3}MLCT and ^{3}IL states and the formation of the excited state equilibrium. Femtosecond transient absorption experiments on compounds **1**−**4** were carried out with excitation at 403 nm, a pump wavelength where MLCT and IL transitions are excited simultaneously (Figure 2B). To resolve individual contributions to the excited-state dynamics from MLCT and IL excitations, fs transient absorption dynamics of **1** were also probed with selective excitation of the MLCT states at 483 nm. However, first the focus will be on the photoexcitation of the compounds at 403 nm, where the photoinduced absorption changes were recorded for delay times up to 1.8 ns.

3.3.1. Femtosecond Transient Absorption of 1−4 in Water upon Excitation at 403 nm. The transient absorption spectra of **1**-**4** recorded at 1 ps after photoexcitation are shown in Figure 5A. All spectra contained contributions from both a GSB and an ESA. In the case of **1** and **2**, the GSB was dominant between 470 and 490 nm, which correlates directly with the MLCT absorption band of these compounds. For **3** and **4**, the GSB was extended to 500 nm, which reflects the bathochromic shift of the ground state MLCT absorption band (Figure 2A).

Figure 5B depicts the temporal evolution of the transient absorption spectra of **1**. The spectra reveal that, in the first 100

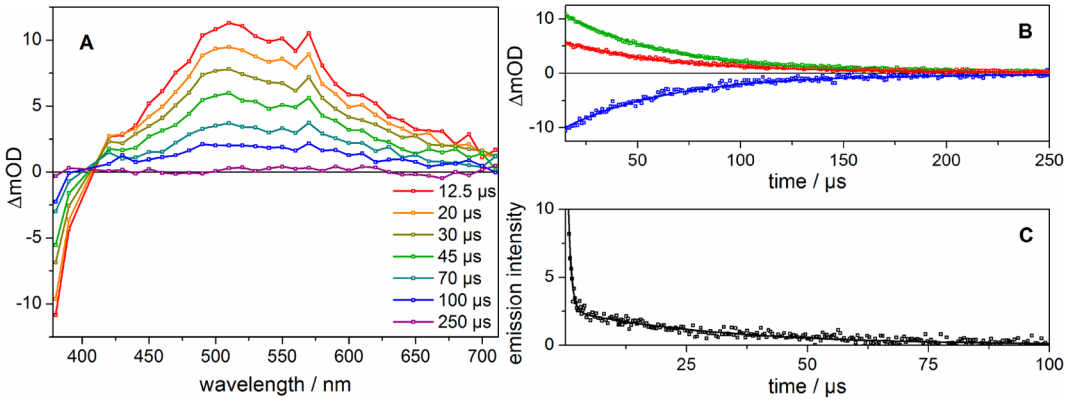

Figure 3. (A) Nanosecond transient absorption spectra recorded for **1** in water upon pumping at 410 nm at different delay times. (B) Kinetic traces of **1** at 380 (blue), 510 (green), and 600 nm (red). (C) Emission decay kinetics recorded for **1** in water at 600 nm pumping at 410 nm. Symbols represent experimental data, while solid lines refer to the fit.

DOI: 10.1021/acs.jpca.5b01737
J. Phys. Chem. A 2015, 119, 3986−3994

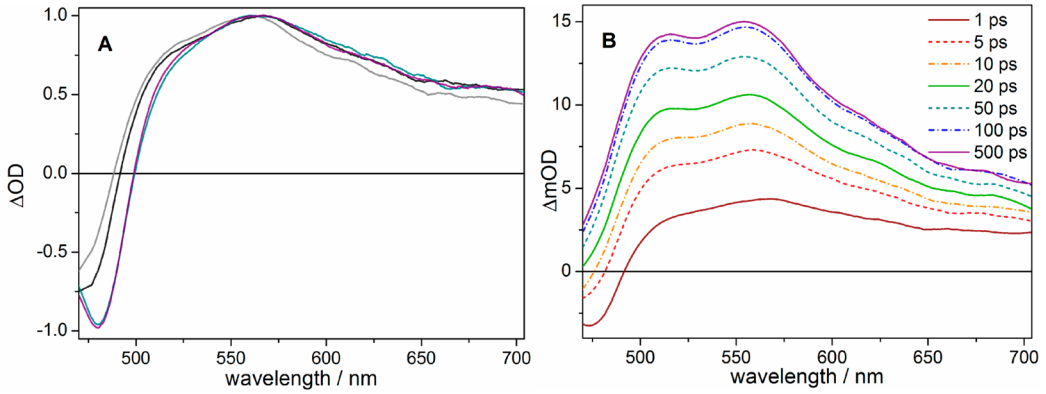

Figure 5. (A) Transient absorption spectra recorded upon pumping at 403 nm at 1 ps for **1** (black), **2** (gray), **3** (cyan), and **4** (violet). Spectra are normalized to the maximum ΔOD signal. (B) Temporal evolution of transient absorption traces for **1** at different delay times upon excitation at 403 nm. At delay times longer than 500 ps, no further changes were observable.

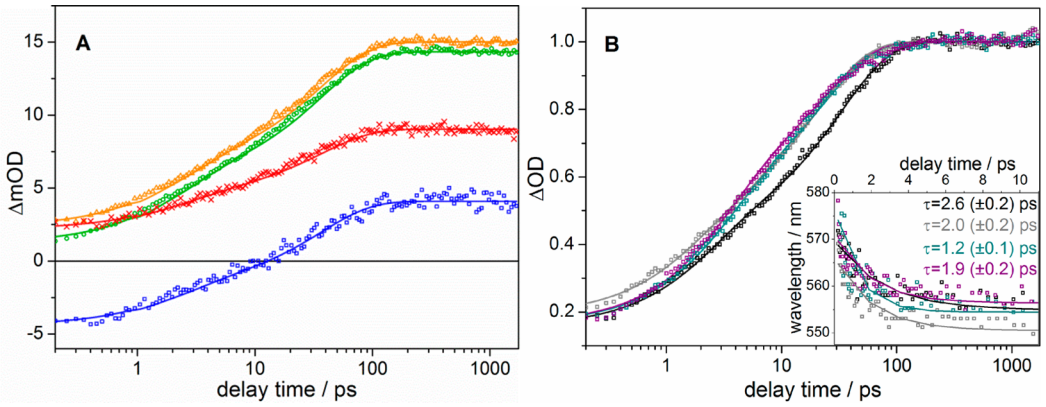

Figure 6. (A) Selected transient absorption traces recorded (λ_{pump} = 403 nm) at 475 (blue), 515 (green), 555 (orange), and 650 nm (red) for **1** in water. Symbols represent experimental data, while solid lines refer to the global fit. (B) Transient absorption kinetics recorded at 555 nm for **1** (black), **2** (gray), **3** (cyan), and **4** (violet). The kinetic traces are normalized to the maximum differential absorption signal at long delay times. Inset shows maxima of transient absorption spectra (symbols) for the first 10 ps after excitation at 403 nm. Lines represent the corresponding monoexponential fit, where time-constants τ are in good agreement with τ_1 from fs transient absorption measurements.

ps after photoexcitation, the transient absorption feature dominating the visible spectral region builds up and remains unchanged for longer delay times. This behavior overwhelmed any negative differential absorption contributions below 500 nm. Consequently, 20 ps after photoexcitation, an all-positive, but spectrally unstructured, differential absorption signal was observed. Only at delay times longer than 10 ps did two distinct maxima of the positive differential absorption band at 516 and 554 nm gradually develop.

Figure 6A shows the kinetics of **1** in water recorded at various probe wavelengths (see the SI for transient absorption kinetics of **2**−**4**). The kinetics reflect the formation of a long-lived ESA within about 200 ps after light absorption, which remains unchanged within the experimentally accessible range of delay times (1.8 ns). Figure 6B compares the transient absorption kinetics of **1**−**4** by plotting the transient kinetics recorded at the maximum of the respective ESA feature at a probe wavelength of 555 nm. All kinetics exhibited similar behavior and reflected the formation of a long-lived excited-state. From the similarity of the transient absorption data of **1**−**4**, it appears that the photoinduced dynamics are dominated by the properties of the ippy-ligand rather than the nature of the coligands employed.

For a quantitative analysis of the transient absorption kinetics, the data were fit with a double-exponential function, and the resultant time constants are summarized in Table 1. For all complexes, a time-constant τ_1 on the order of 2−3 ps was accompanied by a longer time constant τ_2 in the range of 21−33 ps. Sub-100 fs dynamics indicative of ^{1}MLCT → ^{3}MLCT intersystem crossing[52,53] were not resolved, so the initial state in these experiments described in Figure 2B is the ^{3}MLCT state, in which, due to the excitation at 403 nm, the excess charge density is distributed over all coordinating ligands. Hence, the 2−3 ps component, which is spectrally characterized by a blue-shift of the ESA (inset in Figure 6B), has been assigned to localization of the ^{3}MLCT on the ippy-ligand (bearing the energetically lowest-lying orbitals[24]) and subsequent cooling. The process associated with τ_2 is attributed to a rotation about the ip-pyrene coanular bond of the ippy-ligand. This excited-state twist enables electronic coupling between the imidazole and pyrene units and, consequently, the population an IL triplet state via energy transfer. Photoinduced torsional motion, such as rotation about the ip-pyrene bond, should exhibit a viscosity dependence, which can be analyzed with transient absorption spectroscopy in solvents of different viscosity.[33,47,54−57] Such solvent viscosity-dependent dynamics have been observed for Ru(II) polypyridyl complexes bearing 4H-imidazole ligands,[45,47] aryl-substituted bipyridine ligands,[58] and π-conjugated terpyridine systems.[54]

DOI: 10.1021/acs.jpca.5b01737
J. Phys. Chem. A 2015, 119, 3986−3994

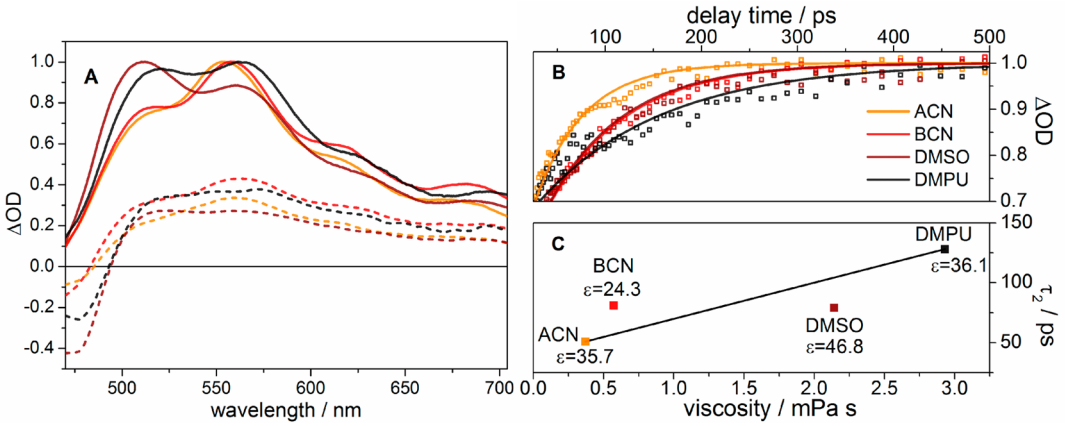

Figure 7. Transient absorption data collected for **1** (λ_{pump} = 403 nm) in ACN (orange), BCN (red), DMSO (brown), and DMPU (black). (A) Transient absorption spectra at 1 (dashed line) and 100 ps (solid line) normalized to the maximum positive ΔOD signal of the 100 ps spectra. (B) Transient absorption traces at 560 nm for all solvents. Symbols represent experimental data, while solid lines refer to the curve obtained from the global fit. The kinetic traces are normalized to the maximum ΔOD signal at long delay times. (C) Dependence of τ_2 on the viscosity and polarity of the solvents.

3.3.2. Viscosity-Dependent Femtosecond Transient Absorption of 1 upon Excitation at 403 nm. Viscosity-dependent fs time-resolved transient absorption measurements of **1** were performed in ACN, BCN, DMSO, and DMPU. The transient spectra of **1** dissolved in these solvents taken at 1 and 100 ps after photoexcitation are summarized in Figure 7A (see the SI for detailed temporal evolution of **1** in the aprotic solvents). In the spectra recorded at 1 ps, a GSB dominated the signal below 500 nm (ACN, BCN/DMSO, and DMPU), in the spectral region of steady-state absorption. At 100 ps all spectra showed positive ΔOD values over the entire probe range with a maximum ΔOD value near 558 nm. This maximum shifted bathochromically upon increasing the viscosity of the solvent. Furthermore, a shoulder at 514 nm was observed in ACN, while for the other solvents, a second maximum at 514 (BCN), 512 (DMSO), and 521 nm (DMPU) was present in the spectra.

The transient absorption kinetics of **1** in different solvents are shown in Figure 7B, and the corresponding time constants used to quantitatively describe the dynamics are listed in Table 2. The kinetics recorded at 560 nm revealed a nonexponential rise of an excited state that reached a maximum ΔOD value at long times over the 500 ps time window investigated. This biexponential buildup of the ESA signal was decelerated in more viscous solvents. Similar to aqueous solutions, the fast component, τ_1 = 1−3 ps, was assigned to the formation of a thermally relaxed, ippy-centered ^{3}MLCT state. The time-constant τ_2 was lengthened with increasing solvent viscosity, reflecting a slower pyrene twist in the more viscous solvents. In ACN (η = 0.39 mPa·s, ε = 35.7) and DMPU (η = 2.93 mPa·s, ε = 36.1) τ_2 was determined to be 51 and 128 ps, respectively, while it was 81 ps in BCN (η = 0.57 mPa·s, ε = 24.3) and 79 ps in DMSO (η = 2.14 mPa·s, ε = 46.8; Figure 7C). The value of τ_2 in DMSO was smaller than expected and can be ascribed to the high polarity of the solvent. Upon planarization of the ippy ligand and formation of the ^{3}IL, the dipole moment of the excited complex is altered and preferentially stabilized by the solvent compared to the ^{3}MLCT. Such solvent stabilization of the ^{3}IL excited state in the highly polar solvent DMSO can be considered to provide additional driving force to populate this state and hence shorten τ_2.

Table 2. Dynamic Viscosity, η, and Dielectric Constant, ε, of Applied Solvents and Time Constants, τ, Measured for 1 in ACN, BCN, DMSO, and DMPU Obtained by Global Fit of Transient Absorption Data with Two Exponential Functions and an Infinite Component

solvent	η/mPa·s,	ε	τ_1/ps	τ_2/ps
ACN	0.39	35.7	2.7	51
BCN	0.57	24.3	1.7	81
DMSO	2.14	46.8	3.3	79
DMPU	2.93	36.1	3.3	128

3.3.3. Femtosecond Transient Absorption of 1 in Water upon Excitation at 483 nm. The previous discussion was based on transient absorption data collected with 403 nm excitation. At this wavelength MLCT states associated with all three coordinating ligands contribute to the absorption of the complex as well as the ippy ligand itself. In order to evaluate the effect of pump wavelength and to disregard contributions from direct $\pi\pi^*$ excitation of the pyrene, transient absorption spectroscopy of **1** was performed in water upon excitation at 483 nm, where primarily the MLCT transitions involving the directly coordinating bpy and phen ligands are excited (see the SI for quantum chemical calculations of contributing excited states). The results (for more detail see the SI) indicated that the kinetics did not change significantly with longer wavelength excitation. However, the underlying photoinduced excited state processes were marginally slowed upon excitation of the complexes at 483 nm compared to excitation at 403 nm. A biexponential global fit afforded time constants of τ_1 = 3.9 and τ_2 = 49 ps, describing the rise of the long-lived excited state. It is possible that the pyrene twist slows as a result of less energy being deposited into the system.

3.3.4. TDDFT Calculation of Pyrene Twist. To obtain insight into the structural relaxation pathways that follow photoexcitation, quantum chemical simulations were carried out for **1**. Excitation in the Franck−Condon region of the singlet ground state (S_0) populates the bright ^{1}MLCT states (S_4 and S_7), which leads to intersystem crossing into the triplet manifold. While several triplet states are accessible with excitation energies matching the S_4 and S_7 states, the T_1 state at 1.89 eV, represented by an electronic configuration where

DOI: 10.1021/acs.jpca.5b01737
J. Phys. Chem. A 2015, 119, 3986−3994

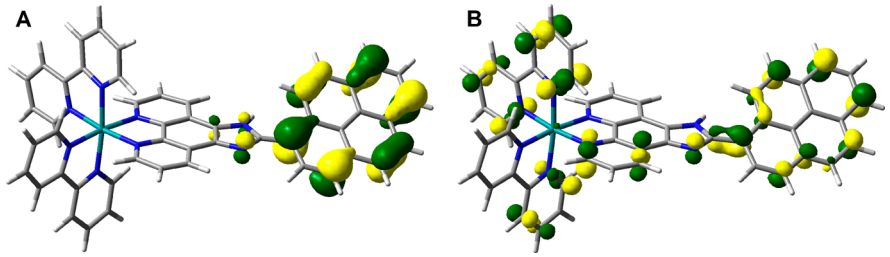

Figure 8. Singly occupied frontier orbitals of (A) $SOMO_1$ and (B) $SOMO_2$ of the T_1 state in its equilibrium geometry.

both unpaired electrons are localized on the ippy ligand, sphere is of particular interest ($SOMO_1$ and $SOMO_2$ in Figure 8). Specifically, the bonding character between the ip and pyrene in $SOMO_2$ was characterized by increased electron density localized at the bond connecting these fragments. A subsequent geometry optimization of the T_1 state at the TDDFT level of theory led to a partial planarization of the ippy ligand from δ = 42.6 (S_0 geometry) to 27.9° (T_1 geometry), accompanied by a slight pyramidalization (9.3°) of the pyrene carbon connected to ip. These geometry alternations markedly lowered the energy of the T_1 state to 1.35 eV, a drop of 0.54 eV. To verify the correlation of the torsion described by the dihedral angle δ and the stabilization of the T_1, a potential energy surface along δ was calculated in the optimized equilibrium structure of T_1 (Figure 9). The potential energy surface of the T_1 state shows a

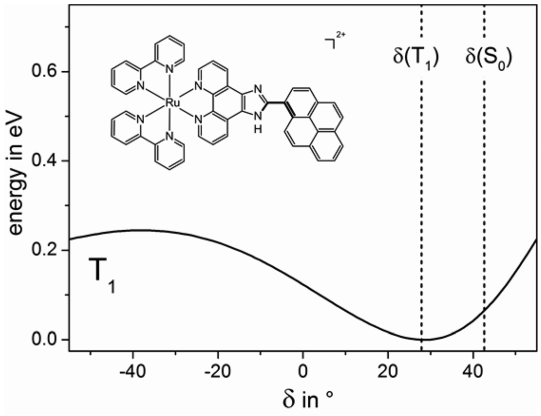

Figure 9. Calculated potential energy surfaces of the T_1 and S_0 states along the torsional angle δ within the optimized equilibrium geometry of the T_1 state. The simulations were performed for $-55° \leq \delta \leq 55°$ with a step size of 1° at the CAM-B3LYP/6-31G(d) level of theory and included the effects of solvation (polarizable continuum model: water).

pronounced dependency on δ, with a stabilization of approximately 0.1 eV between the S_0 geometry and the T_1 equilibrium geometry. Hence, TDDFT simulations point to a population of the lowest triplet state following photoexcitation to ^{1}MLCT states, leading to partial planarization of the ippy ligand by twist of the pyrene ligand with respect to the ip ring system.

Figure 10 summarizes the relaxation processes observed for **1**−**4** inferred from both ns and fs transient absorption experiments. Picosecond dynamics (derived from fs measurements) were characterized by vibrational relaxation within the ^{3}MLCT manifold followed by rotation about the pyrene-ip bond, enabling population of the ^{3}IL state. The final ground-state recovery was observed on the microsecond timescale.

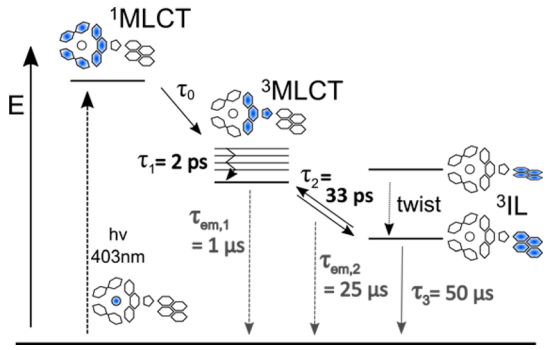

Figure 10. Schematic representation of the relative energetic positions of the excited states involved in the picosecond excited state dynamics.

4. CONCLUSION

The photophysics of a series of Ru(II) dyads bearing the ippy ligand have been investigated with transient absorption and time-resolved emission spectroscopy. The picosecond dynamics were best described through vibrational relaxation centered on the ippy ligand and subsequent torsional motion of the pyrene system, which facilitates energy transfer from the thermalized ^{3}MLCT state to the ^{3}IL (pyrene) state. Despite differing coligands, similar excited state dynamics were observed for **1**−**4**, suggesting that the kinetics are influenced primarily by the ippy ligand. Transient absorption on the μs timescale and emission experiments indicated a nonradiative ground state recovery from the ^{3}IL state and two emission lifetimes, which were assigned to spontaneous and delayed emission of the ^{3}MLCT state. The time constants of 24 (long-lived emission) and 46 μs (transient absorption) suggest an equilibrium between ^{3}MLCT and ^{3}IL states, which explains the long-lived τ_2 emission with ^{3}MLCT character.

These spectroscopic results are useful in understanding the utility of Ru(II) dyads as PDT agents. As previously demonstrated, the same structural features that give rise to these low-lying, ligand-centered states also establish high affinity toward biomolecules such as DNA. For example, the lipophilic pyrene handle is an excellent DNA intercalating unit, ensuring maximal photodamage to the DNA helix due to strong binding coupled with efficient excited-state charge distribution over the intercalating ippy ligand. The energetic proximity of the pyrene-localized ^{3}IL state prolongs the lifetime of the ^{3}MLCT state (observable by delayed emission) and also contributes a dark state of ^{3}IL character with the longest lifetime τ_3 (observable by transient absorption) that could mediate photoactivity toward biological targets. We conclude that low-lying, long-lived ^{3}IL states are influential in Ru(II) ippy dyads, resulting in excited states that are highly photosensitizing for destroying unwanted cells upon visible light activation. It is interesting to speculate that binding to biological targets may

DOI: 10.1021/acs.jpca.5b01737
J. Phys. Chem. A 2015, 119, 3986−3994

exert a templating effect that planarizes the ip-pyrene unit and facilitates ^{3}IL population, increasing the photoreactivity of the dyads beyond what is possible from conventional ^{3}MLCT states. To our knowledge this is the first investigation to probe the relationship between torsional motion and ^{3}IL state access in metal−organic dyads. Studies are underway to examine the effects of DNA binding on the excited state photophysical model outlined herein.

■ ASSOCIATED CONTENT

Supporting Information

Acid−base titration experiments, calculated absorption spectra (including vertical excitation energies and molecular orbital images of most relevant configurations), femtosecond transient absorption spectra and decay traces in water using a pump wavelength of 403 nm, femtosecond transient absorption spectra and decay traces in organic, aprotic solvents (ACN, BCN, DMSO, and DMPU) using a pump wavelength of 403 nm, and femtosecond transient absorption spectra and decay traces in water using a pump wavelength of 483 nm. This material is available free of charge via the Internet at http://pubs.acs.org.

■ AUTHOR INFORMATION

Corresponding Authors

*Tel.: (902) 585-1320. Fax: (902) 585-1114. E-mail: sherri.mcfarland@acadiau.ca.

*Tel.: +49 (0)3641 206-332. Fax: +49 (0)3641 206-399. E-mail: benjamin.dietzek@ipht-jena.de.

Notes

The authors declare no competing financial interest.

■ ACKNOWLEDGMENTS

B.D. thanks the Fonds der Chemischen Industrie and a Landesgraduiertenstipendium to C.R. for support, and S.A.M. acknowledges financial support from the Natural Sciences and Engineering Council of Canada, the Canadian Foundation for Innovation, the Nova Scotia Research and Innovation Trust, and Acadia University.

■ REFERENCES

(1) Welter, S.; Brunner, K.; Hofstraat, J. W.; De Cola, L. Electroluminescent Device with Reversible Switching between Red and Green Emission. *Nature* **2003**, *421*, 54−57.

(2) Mobian, P.; Kern, J.-M.; Sauvage, J.-P. Light-Driven Machine Prototypes Based on Dissociative Excited States: Photoinduced Decoordination and Thermal Recoordination of a Ring in a Ruthenium(II)-Containing [2]Catenane. *Angew. Chem., Int. Ed.* **2004**, *43*, 2392−2395.

(3) Balzani, V.; Bergamini, G.; Marchioni, F.; Ceroni, P. Ru(II)-Bipyridine Complexes in Supramolecular Systems, Devices and Machines. *Coord. Chem. Rev.* **2006**, *250*, 1254−1266.

(4) Grätzel, M. Dye-Sensitized Solar Cells. *J. Photochem. Photobiol. C* **2003**, *4*, 145−153.

(5) Wang, P.; Zakeeruddin, S. M.; Moser, J. E.; Nazeeruddin, M. K.; Sekiguchi, T.; Grätzel, M. A Stable Quasi-Solid-State Dye-Sensitized Solar Cell with an Amphiphilic Ruthenium Sensitizer and Polymer Gel Electrolyte. *Nat. Mater.* **2003**, *2*, 402−407.

(6) Chen, C.-Y.; et al. Highly Efficient Light-Harvesting Ruthenium Sensitizer for Thin-Film Dye-Sensitized Solar Cells. *ACS Nano* **2009**, *3*, 3103−3109.

(7) Tschierlei, S.; Karnahl, M.; Presselt, M.; Dietzek, B.; Guthmuller, J.; González, L.; Schmitt, M.; Rau, S.; Popp, J. Photochemical Fate: The First Step Determines Efficiency of H_2 Formation with a Supramolecular Photocatalyst. *Angew. Chem., Int. Ed.* **2010**, *49*, 3981−3984.

(8) Andreiadis, E. S.; Chavarot-Kerlidou, M.; Fontecave, M.; Artero, V. Artificial Photosynthesis: From Molecular Catalysts for Light-Driven Water Splitting to Photoelectrochemical Cells. *Photochem. Photobiol.* **2011**, *87*, 946−964.

(9) Kärkäs, M. D.; Verho, O.; Johnston, E. V.; Åkermark, B. Artificial Photosynthesis: Molecular Systems for Catalytic Water Oxidation. *Chem. Rev.* **2014**, *114*, 11863.

(10) Sun, L.; Hammarström, L.; Åkermark, B.; Styring, S. Towards Artificial Photosynthesis: Ruthenium−manganese Chemistry for Energy Production. *Chem. Soc. Rev.* **2001**, *30*, 36−49.

(11) Lippitsch, M. E.; Pusterhofer, J.; Leiner, M. J. P.; Wolfbeis, O. S. Fibre-Optic Oxygen Sensor with the Fluorescence Decay Time as the Information Carrier. *Anal. Chim. Acta* **1988**, *205*, 1−6.

(12) Demas, J. N.; DeGraff, B. A. Design and Applications of Highly Luminescent Transition Metal Complexes. *Anal. Chem.* **1991**, *63*, 829A−837A.

(13) Demas, J. N.; DeGraff, B. A. Applications of Luminescent Transition Metal Complexes to Sensor Technology and Molecular Probes. *J. Chem. Educ.* **1997**, *74*, 690.

(14) Velders, A. H.; Kooijman, H.; Spek, A. L.; Haasnoot, J. G.; de Vos, D.; Reedijk, J. Strong Differences in the in Vitro Cytotoxicity of Three Isomeric Dichlorobis(2-phenylazopyridine)ruthenium(II) Complexes. *Inorg. Chem.* **2000**, *39*, 2966−2967.

(15) Clarke, M. J. Ruthenium Metallopharmaceuticals. *Coord. Chem. Rev.* **2002**, *232*, 69−93.

(16) Szacilowski, K.; Macyk, W.; Drzewiecka-Matuszek, A.; Brindell, M.; Stochel, G. Bioinorganic Photochemistry: Frontiers and Mechanisms. *Chem. Rev.* **2005**, *105*, 2647−2694.

(17) Ostrowski, A. D.; Ford, P. C. Metal Complexes as Photochemical Nitric Oxide Precursors: Potential Applications in the Treatment of Tumors. *Dalton Trans.* **2009**, 10660−10669.

(18) Crespy, D.; Landfester, K.; Schubert, U. S.; Schiller, A. Potential Photoactivated Metallopharmaceuticals: From Active Molecules to Supported Drugs. *Chem. Commun.* **2010**, *46*, 6651−6662.

(19) Wachter, E.; Heidary, D. K.; Howerton, B. S.; Parkin, S.; Glazer, E. C. Light-Activated Ruthenium Complexes Photobind DNA and Are Cytotoxic in the Photodynamic Therapy Window. *Chem. Commun.* **2012**, *48*, 9649.

(20) Dougherty, T. J.; Gomer, C. J.; Henderson, B. W.; Jori, G.; Kessel, D.; Korbelik, M.; Moan, J.; Peng, Q. Photodynamic Therapy. *J. Natl. Cancer Inst.* **1998**, *90*, 889−905.

(21) Macdonald, I. J.; Dougherty, T. J. Basic Principles of Photodynamic Therapy. *J. Porphyrins Phthalocyanines* **2001**, *5*, 105−129.

(22) Dolmans, D. E. J. G. J.; Fukumura, D.; Jain, R. K. Photodynamic Therapy for Cancer. *Nat. Rev. Cancer* **2003**, *3*, 380−387.

(23) Farrer, N. J.; Salassa, L.; Sadler, P. J. Photoactivated Chemotherapy (PACT): The Potential of Excited-State D-Block Metals in Medicine. *Dalton Trans.* **2009**, 10690.

(24) Stephenson, M.; et al. Ru(II) Dyads Derived from 2-(1-Pyrenyl)-1H-imidazo[4,5-f][1,10]phenanthroline: Versatile Photosensitizers for Photodynamic Applications. *J. Phys. Chem. A* **2014**, *118*, 10507−10521.

(25) Omary, M. A.; Kassab, R. M.; Haneline, M. R.; Elbjeirami, O.; Gabbaï, F. P. Enhancement of the Phosphorescence of Organic Luminophores upon Interaction with a Mercury Trifunctional Lewis Acid. *Inorg. Chem.* **2003**, *42*, 2176−2178.

(26) Lincoln, R.; et al. Exploitation of Long-Lived ^{3}IL Excited States for Metal−Organic Photodynamic Therapy: Verification in a Metastatic Melanoma Model. *J. Am. Chem. Soc.* **2013**, *135*, 17161−17175.

(27) Ji, S.; Wu, W.; Wu, W.; Guo, H.; Yang, Q.; Wang, Q.; Zhang, X.; Wu, Y.; Zhao, J. Synthesis of Polypyridyl Ruthenium Complexes with 2-(1-Aryl)-1H-imidazo[4,5-F]-1,10-Phenanthroline Ligand and Its Application for Luminescent Oxygen Sensing. *Front. Chem. China* **2010**, *5*, 193−199.

DOI: 10.1021/acs.jpca.5b01737
J. Phys. Chem. A 2015, 119, 3986−3994

(28) Wyld, L.; Reed, M. W.; Brown, N. J. The Influence of Hypoxia and pH on Aminolaevulinic Acid-Induced Photodynamic Therapy in Bladder Cancer Cells in Vitro. *Br. J. Cancer* **1998**, *77*, 1621−1627.
(29) Tanielian, C.; Schweitzer, C.; Mechin, R.; Wolff, C. Quantum Yield of Singlet Oxygen Production by Monomeric and Aggregated Forms of Hematoporphyrin Derivative. *Free Radic. Biol. Med.* **2001**, *30*, 208−212.
(30) Friedman, A. E.; Chambron, J. C.; Sauvage, J. P.; Turro, N. J.; Barton, J. K. A Molecular Light Switch for DNA: $Ru(bpy)_2(dppz)^{2+}$. *J. Am. Chem. Soc.* **1990**, *112*, 4960−4962.
(31) Olson, E. J. C.; Hu, D.; Hörmann, A.; Jonkman, A. M.; Arkin, M. R.; Stemp, E. D. A.; Barton, J. K.; Barbara, P. F. First Observation of the Key Intermediate in the "Light-Switch" Mechanism of $[Ru(phen)_2dppz]^{2+}$. *J. Am. Chem. Soc.* **1997**, *119*, 11458−11467.
(32) Brennaman, M. K.; Meyer, T. J.; Papanikolas, J. M. $[Ru(bpy)_2dppz]^{2+}$ Light-Switch Mechanism in Protic Solvents as Studied through Temperature-Dependent Lifetime Measurements. *J. Phys. Chem. A* **2004**, *108*, 9938−9944.
(33) Siebert, R.; Akimov, D.; Schmitt, M.; Winter, A.; Schubert, U. S.; Dietzek, B.; Popp, J. Spectroscopic Investigation of the Ultrafast Photoinduced Dynamics in Π-Conjugated Terpyridines. *ChemPhysChem* **2009**, *10*, 910−919.
(34) Karnahl, M.; Kuhnt, C.; Ma, F.; Yartsev, A.; Schmitt, M.; Dietzek, B.; Rau, S.; Popp, J. Tuning of Photocatalytic Hydrogen Production and Photoinduced Intramolecular Electron Transfer Rates by Regioselective Bridging Ligand Substitution. *ChemPhysChem* **2011**, *12*, 2101−2109.
(35) Lee, C.; Yang, W.; Parr, R. G. Development of the Colle-Salvetti Correlation-Energy Formula into a Functional of the Electron Density. *Phys. Rev. B* **1988**, *37*, 785−789.
(36) Becke, A. D. Density-functional Thermochemistry. III. The Role of Exact Exchange. *J. Chem. Phys.* **1993**, *98*, 5648−5652.
(37) Guthmuller, J.; Champagne, B. Time Dependent Density Functional Theory Investigation of the Resonance Raman Properties of the Julolidinemalononitrile Push-Pull Chromophore in Various Solvents. *J. Chem. Phys.* **2007**, *127*, 164507.
(38) Becke, A. D. Density-Functional Exchange-Energy Approximation with Correct Asymptotic Behavior. *Phys. Rev. A* **1988**, *38*, 3098−3100.
(39) Yanai, T.; Tew, D. P.; Handy, N. C. A New Hybrid Exchange−correlation Functional Using the Coulomb-Attenuating Method (CAM-B3LYP). *Chem. Phys. Lett.* **2004**, *393*, 51−57.
(40) Andrae, D.; Häußermann, U.; Dolg, M.; Stoll, H.; Preuß, H. Energy-Adjustedab Initio Pseudopotentials for the Second and Third Row Transition Elements. *Theor. Chim. Acta* **1990**, *77*, 123−141.
(41) Hariharan, P. C.; Pople, J. A. The Influence of Polarization Functions on Molecular Orbital Hydrogenation Energies. *Theor. Chim. Acta* **1973**, *28*, 213−222.
(42) Brown, R. G.; Entwistle, N.; Hepworth, J. D.; Hodgson, K. W.; May, B. Photophysics of Three Pyridylbenzimidazoles in Solution. *J. Phys. Chem.* **1982**, *86*, 2418−2420.
(43) Beckert, R.; Hipyius, C.; Gebauer, T.; Stöckner, F.; Lüdigk, C.; Weiss, D.; Raabe, D.; Günther, W.; Görls, H. Syntheses and Properties of Cycloamidines Based on 4H-Imidazoles. *Z. Naturforsch., B: J. Chem. Sci.* **2006**, *61*, 437−447.
(44) Montero, R.; Conde, Á. P.; Ovejas, V.; Fernández-Fernández, M.; Castaño, F.; Longarte, A. Ultrafast Evolution of Imidazole after Electronic Excitation. *J. Phys. Chem. A* **2012**, *116*, 10752−10758.
(45) Kupfer, S.; Guthmuller, J.; Wächtler, M.; Losse, S.; Rau, S.; Dietzek, B.; Popp, J.; González, L. Protonation Effects on the Resonance Raman Properties of a Novel (terpyridine)Ru(4H-Imidazole) Complex: An Experimental and Theoretical Case Study. *Phys. Chem. Chem. Phys.* **2011**, *13*, 15580−15588.
(46) Bhaumik, C.; Saha, D.; Das, S.; Baitalik, S. Synthesis, Structural Characterization, Photophysical, Electrochemical, and Anion-Sensing Studies of Luminescent Homo- and Heteroleptic Ruthenium(II) and Osmium(II) Complexes Based on Terpyridyl-Imidazole Ligand. *Inorg. Chem.* **2011**, *50*, 12586−12600.
(47) Wächtler, M.; Kupfer, S.; Guthmuller, J.; Rau, S.; González, L.; Dietzek, B. Structural Control of Photoinduced Dynamics in 4H-Imidazole-Ruthenium Dyes. *J. Phys. Chem. C* **2012**, *116*, 25664−25676.
(48) Kulkarni, M. S.; Madhava Rao, B. S.; Sastri, C. V.; Maiya, B. G.; Mohan, H.; Mittal, J. P. Redox Chemistry of Ru(II) Complexes of 6,7-Dicyanodipyridoquinoxaline: A Radiation Chemical Study. *J. Photochem. Photobiol. Chem.* **2004**, *167*, 101−109.
(49) Jing, B.; Zhang, M.; Shen, T. $[Ruthenium(II)(bpy)2L]^{2+}$, Where L Are Imidazo[f]-1,10-Phenanthrolines: Synthesis, Photophysics and Binding with DNA. *Spectrochim. Acta. A* **2004**, *60*, 2635−2641.
(50) Wang, X.; Del Guerzo, A.; Schmehl, R. H. Photophysical Behavior of Transition Metal Complexes Having Interacting Ligand Localized and Metal-to-Ligand Charge Transfer States. *J. Photochem. Photobiol. C* **2004**, *5*, 55−77.
(51) Yin, H.; Stephenson, M.; Gibson, J.; Sampson, E.; Shi, G.; Sainuddin, T.; Monro, S.; McFarland, S. A. In Vitro Multiwavelength PDT with ^{3}IL States: Teaching Old Molecules New Tricks. *Inorg. Chem.* **2014**, *53*, 4548−4559.
(52) Damrauer, N. H.; Cerullo, G.; Yeh, A.; Boussie, T. R.; Shank, C. V.; McCusker, J. K. Femtosecond Dynamics of Excited-State Evolution in $[Ru(bpy)_3]^{2+}$. *Science* **1997**, *275*, 54−57.
(53) Cannizzo, A.; van Mourik, F.; Gawelda, W.; Zgrablic, G.; Bressler, C.; Chergui, M. Broadband Femtosecond Fluorescence Spectroscopy of [Ru(bpy)3]2+. *Angew. Chem.* **2006**, *118*, 3246−3248.
(54) Siebert, R.; Winter, A.; Schubert, U. S.; Dietzek, B.; Popp, J. Excited-State Planarization as Free Barrierless Motion in a Π-Conjugated Terpyridine. *J. Phys. Chem. C* **2010**, *114*, 6841−6848.
(55) Bagchi, B. Isomerization Dynamics in Solution. *Int. Rev. Phys. Chem.* **1987**, *6*, 1−33.
(56) Dietzek, B.; Tarnovsky, A. N.; Yartsev, A. Visualizing Overdamped Wavepacket Motion: Excited-State Isomerization of Pseudocyanine in Viscous Solvents. *Chem. Phys.* **2009**, *357*, 54−62.
(57) Singh, C.; Modak, B.; Mondal, J. A.; Palit, D. K. Ultrafast Twisting Dynamics in the Excited State of Auramine. *J. Phys. Chem. A* **2011**, *115*, 8183−8196.
(58) Meylemans, H. A.; Hewitt, J. T.; Abdelhaq, M.; Vallett, P. J.; Damrauer, N. H. Exploiting Conformational Dynamics To Facilitate Formation and Trapping of Electron-Transfer Photoproducts in Metal Complexes. *J. Am. Chem. Soc.* **2010**, *132*, 11464−11466.

DOI: 10.1021/acs.jpca.5b01737
J. Phys. Chem. A 2015, 119, 3986−3994